Check for updates

α2-Adrenergic modulation of I_h in adult-born granule cells in the olfactory bulb

Ruilong Hu†, Janam Shankar†, Grant Z. Dong, Pablo S. Villar and Ricardo C. Araneda*

Department of Biology, University of Maryland, College Park, College Park, MD, United States

In the olfactory bulb (OB), a large population of axon-less inhibitory interneurons, the granule cells (GCs), coordinate network activity and tune the output of principal neurons, the mitral and tufted cells (MCs), through dendrodendritic interactions. Furthermore, GCs undergo neurogenesis throughout life, providing a source of plasticity to the neural network of the OB. The function and integration of GCs in the OB are regulated by several afferent neuromodulatory signals, including noradrenaline (NA), a state-dependent neuromodulator that plays a crucial role in the regulation of cortical function and task-specific decision processes. However, the mechanisms by which NA regulates GC function are not fully understood. Here, we show that NA modulates hyperpolarization-activated currents (I_h) *via* the activation of α2-adrenergic receptors (ARs) in adult-born GCs (abGCs), thus directly acting on channels that play essential roles in regulating neuronal excitability and network oscillations in the brain. This modulation affects the dendrodendritic output of GCs leading to an enhancement of lateral inhibition onto the MCs. Furthermore, we show that NA modulates subthreshold resonance in GCs, which could affect the temporal integration of abGCs. Together, these results provide a novel mechanism by which a state-dependent neuromodulator acting on I_h can regulate GC function in the OB.

KEYWORDS

dendrodendritic, lateral inhibition, neurogenesis, noradrenaline, olfactory bulb

Introduction

The precise regulation of inhibitory circuits is an inherent component of sensory processing (Lledo et al., 2005; Isaacson and Scanziani, 2011; Griffen and Maffei, 2014). In the olfactory bulb (OB), the GABAergic granule cells (GCs) comprise the largest population of inhibitory neurons (Lledo et al., 2006; Lepousez et al., 2013). A major functional role of GCs is the recurrent and lateral inhibition of output neurons, the mitral and tufted cells (MCs, herein) *via* dendrodendritic synapses (Jahr and Nicoll, 1980; Isaacson and Strowbridge, 1998). Through these interactions with MCs, GCs

are thought to facilitate network oscillations and decorrelation of principal neurons allowing for discrimination of similar odor patterns (Lepousez and Lledo, 2013; Fukunaga et al., 2014; Gschwend et al., 2015; Wanner and Friedrich, 2020). GC activity is regulated by several cell-intrinsic and -extrinsic mechanisms, including excitatory feedback from higher olfactory areas, and several neuromodulatory centers, underscoring their important role in the modulation of MC output and odor processing (Schoppa and Westbrook, 1999; Schoppa and Urban, 2003; Fletcher and Chen, 2010; Boyd et al., 2012; Markopoulos et al., 2012; Stroh et al., 2012; Otazu et al., 2015).

Notably, GCs are continuously born throughout life in a process known as adult neurogenesis (Altman, 1962; Altman and Das, 1965). Thus, the dendrodendritic synapses in the OB undergo constant remodeling (Lois and Alvarez-Buylla, 1994; Petreanu and Alvarez-Buylla, 2002). During their integration, adult-born GCs' (abGCs) dendrites arborize and form functional synaptic contacts with the local circuit and undergo an activity-dependent critical period that affects synaptic connectivity and cell survival (Petreanu and Alvarez-Buylla, 2002; Carleton et al., 2003; Lledo et al., 2006). These changes are accompanied by age-dependent expression of ion channels which ensures their coordinated integration in the OB circuit (Belluzzi et al., 2003; Carleton et al., 2003; Lledo et al., 2006). Although the molecular mechanisms underlying the functional integration of abGCs are not fully understood, this process appears to be highly regulated by both local and afferent synaptic inputs (Lepousez et al., 2015).

A key regulator of both dendrodendritic inhibition (DDI) and the functional integration of abGCs is noradrenaline (NA), released from broadly projecting neurons of the locus coeruleus (Jahr and Nicoll, 1982; Veyrac et al., 2009; Fletcher and Chen, 2010; Moreno et al., 2012). For example, pharmacological blockade of adrenergic receptors (ARs) in the OB has been shown to impair task-dependent survival of abGCs (Veyrac et al., 2009; Moreno et al., 2012), suggesting that NA affects abGC physiology as early as their critical period of integration. However, the cellular mechanisms underlying the adrenergic regulation of abGC physiology and integration during, and past, the critical period remain poorly understood. NA has been shown to regulate neuronal excitability and network dynamics through a cAMP-dependent hyperpolarization-activated current, I_h (Lüthi and McCormick, 1998; Berridge and Waterhouse, 2003; Sara, 2009), through the alteration of intracellular cAMP levels *via* α_2- or β-ARs. In previous work, we showed that GCs born just after birth express I_h, that this current could influence intrinsic excitability of GCs, and exhibited cAMP responses properties that indicated the presence of HCN1, 2, or 4 subunits (Hu et al., 2016). However, the presence of I_h in abGCs and its regulation by NA in the OB have not been studied.

Here, using whole-cell patch clamp electrophysiology, we show that several physiological parameters that control neuronal excitability of abGCs show a progressive change during integration, which extends well beyond the critical period. Importantly, I_h is present in abGCs, and the size of this current increases throughout their maturation. In addition, we show that activation of α_2-ARs suppresses I_h *via* a cAMP-dependent mechanism. Suppression of I_h increases dendritic excitability, thereby enhancing lateral inhibition onto MCs. Furthermore, we show that α_2-AR activation modulated the I_h-dependent resonance in GCs. Together these findings suggest that α_2-AR modulation of I_h in abGCs may impart unique features toward fine-tuning interactions of local GABAergic circuits with the OB output neurons in a state-dependent manner.

Materials and methods

Animals

All experiments were conducted following the guidelines of the IACUC of the University of Maryland. Experiments were performed on both adult male and female wild-type (C57/BL6) or Thy1-ChR2 (Jackson Laboratory: stock #007612) mice 2–6 months of age, from breeding pairs housed in our animal facility.

Stereotaxic viral injections

To label abGCs, mice (P40–P50) were injected with 200 nL of AAV5-Syn-GFP (Addgene) in the rostral migratory stream (RMS), using the following stereotaxic coordinates (in mm): DV −2.85, ML ± 0.8, AP +3.3. Anesthetized C57/BL6 mice (2% isoflurane) were head-fixed in a stereotaxic apparatus (Kopf, catalog #940) and a 33-gauge needle (5 μL syringe, Hamilton) was inserted through a 1 mm craniotomy. The speed of virus injection (200 nL/min) was controlled using a syringe pump (Micro4 Microsyringe pump, World Precision Instruments). During the surgery, eyes were lubricated with a petrolatum ophthalmic ointment (Paralube) and body temperature was maintained using a heating pad. An intraperitoneal injection of carprofen (5 mg/kg) was used as an analgesic.

Histology and confocal imaging

To characterize the morphological characteristic of abGCs, RMS-injected mice were transcardially perfused with cold 4% PFA diluted in 0.1 M PBS, pH 7.4. Brains were then harvested and postfixed overnight at 4°C in the same fixative. Brains were sliced in sections of 100 μm using a vibratome (Leica VT1000). Nuclei were stained with DAPI (Invitrogen) and mounted in a solution of Mowiol-DABCO, prepared as previously described (Villar et al., 2021). Images were acquired using a Leica SP5X confocal microscope (Leica Microsystems) and processed using ImageJ (National Institute of Health).

Electrophysiology slice preparation

Experiments were performed in OB slices using methods previously described (Hu et al., 2016). Briefly, sagittal or horizontal OB slices were prepared in an oxygenated ice-cold artificial cerebrospinal fluid (ACSF) containing lower Ca^{2+} (0.5 mM) and higher Mg^{2+} (6 mM) compared to normal ACSF. Sections (250 μm) were obtained using a vibratome (Leica VT1000) and then transferred to an incubation chamber containing normal ACSF (see below) and left to recuperate for at least 30 min at 35°C, before the recordings. In all experiments, the extracellular solution is ACSF of the following composition (in mM): 125 NaCl, 26 $NaHCO_3$, 1.25 NaH_2PO_4, 2.5 KCl, 2 $CaCl_2$, 1 $MgCl_2$, 1 myo-inositol, 0.4 ascorbic acid, 2 Na-pyruvate, and 15 glucose, continuously oxygenated (95% O_2–5% CO_2).

Recordings and data analysis

Neurons were visualized using an Olympus BX51W1 microscope and recorded using a dual EPC10 amplifier interfaced with the PatchMaster software (HEKA, Harvard Bioscience). Whole-cell recordings were performed at room temperature (∼21°C) or at 32 ± 2°C, using the TC-342B Automatic Temperature Controller (Warner Instruments, Hamden, CT) with a perfusion speed of 2–3 mL/min, using standard patch pipettes (2–8 MΩ resistance). For current-clamp recording, the internal solution had the following composition (in mM): 130 K-gluconate, 4 KCl, 10 HEPES-K, 10 Na phosphocreatine, 2 Na-ATP, 4 Mg-ATP, and 0.3 GTP adjusted to pH 7.3 with KOH (∼290–305 mOsm). For MC voltage-clamp recordings, the K-gluconate was substituted with Cs-gluconate or CsCl. In some of the recordings, the dye Alexa Fluor 594 (20 μM, Invitrogen) was included in the internal recording solution for morphological validation and reconstruction of the recorded neurons.

All electrophysiological recordings were analyzed in MATLAB (Mathworks). Although the whole-cell configuration precludes an accurate measurement of the resting membrane potential (V_m) due to the cell's dialysis with the pipette's internal solution, we estimated V_m right after rupturing the seal. The properties of I_h were measured as previously described (Hu et al., 2016). Activation kinetics (τ) were determined by fitting a single exponential function to the current trace when stepping from –60 to –130 mV. Voltage dependency was calculated by fitting the tail-current values to a Boltzmann function of the following form: $I = I_{max}/\{1 + \exp[(V - V_{half})/k_s]\}$, where I_{max} is the maximal current, V is the prepulse potential, V_{half} is the half-activation potential of the current, and k_s is the slope factor. Statistical significance was determined by Student's t-test, Kolmogorov–Smirnov test, or one-way ANOVA. Subthreshold resonance was measured using a standard impedance amplitude protocol (ZAP), in which a stimulus of sinusoidal current of constant amplitude and exponentially increasing frequency (0.2–20 Hz) is injected into the cell. The ZAP protocol was obtained at –75 mV. The impedance profile was calculated as the magnitude of the ratio of the fast Fourier transforms of the voltage response and current input (Gutfreund et al., 1995; Hutcheon and Yarom, 2000; Vera et al., 2014), using the following equation: Z (f) = |FFT[V(t)]/FFT[I(t)]|. The exponential ZAP protocol we employed works best on cells with lower resonant frequencies (1–4 Hz). The impedance profile was smoothed, and the resonant frequency (f_{res}) was determined as the frequency at which the maximal impedance value occurred. The strength of resonance (Q factor) was calculated as the ratio between the maximal impedance (| $Z(f_{res})$|) and the lowest frequency impedance values (| $Z(f_{low})$|; 0.5 Hz). A neuron was considered resonant if $f_{res} > f_{low}$ and Q > 1.01. Previous work in rat brain slices has demonstrated a low success rate in eliciting lateral inhibition in paired MC recordings (4 in 40 pairs) (Isaacson and Strowbridge, 1998). Our success rate was 4 in 94 pairs from adult mouse brain slices; therefore, we opted for using an optogenetic approach. For ChR2 stimulation with Thy1-ChR2 brain slices, a 40x objective (Olympus) was used and focused over the MC layer or shifted laterally along the MC layer to locally activate MCs. Statistical significance was determined by Student's t-test.

Pharmacological agents

Drugs were included in the bathing solution and perfused at a speed of ∼3 mL/min: 4-(N-ethyl-N-phenylamino)-1, 2-dimethyl-6-(methylamino) pyrimidinium chloride (ZD7288), 8-(4-chloro-phenylthio)-2-O-methyladenosine-3,5-cyclic monophosphate (8-CPT-cAMP), N-(2,6-dichlorophenyl)-4,5-dihydro-1H-imidazol-2-amine hydrochloride (clonidine, Clon), 6-cyano-7-nitroquinoxaline-2,3-dione disodium,6-Imino-3-(4-methoxyphenyl)-1 (6H)-pyridazinebutanoic acid hydrobromide (gabazine, GBZ), and tetrodotoxin (TTX). All drugs were purchased from Tocris (Bio-Techne), except for 8-CPT-cAMP (Abcam).

Results

Intrinsic and extrinsic excitability of adult-born granule cells exhibit changes beyond their critical period of integration

To investigate the neurophysiological properties of abGCs during the critical period of their functional integration, we

expressed the fluorescent marker GFP in abGCs using viral injections in the RMS of adult mice (see section "Materials and methods"). We recorded abGCs at two time points: 2 and 6 weeks post-injection (2 and 6 weeks old, respectively). Previous studies have shown that during this time window abGCs make functional connections with the pre-existing circuit; at 2 weeks, GCs are undergoing a critical period of synaptic remodeling, whereas cells at 6 weeks are considered to be fully integrated (Petreanu and Alvarez-Buylla, 2002; Lledo et al., 2006; Lepousez et al., 2013). Two weeks post-injection, abGCs exhibit mature morphological characteristics, including a primary apical dendrite, along with distal branches and prominent spines, with 53% of abGCs corresponding to class V, 37% to class IV, and 10% to class III, as previously described (class V, 41/78; class IV, 29/78; class III, 8/78; $n = 3$ mice; **Figure 1A**; Petreanu and Alvarez-Buylla, 2002; Carleton et al., 2003). Interestingly, despite the degree of maturation exhibited by abGCs at 2 weeks, they continued to exhibit significant changes in excitability as they further matured. Specifically, the resting membrane potential (RMP) and input resistance were significantly different between these two age groups. At 2 weeks, abGCs had a more depolarized RMP than at 6 weeks (-67.9 ± 1.2 mV, 2 weeks, $n = 16$ cells; -73.1 ± 1.1 mV, 6 weeks; $n = 18$ cells; $p = 0.003$; **Figure 1B**) and had a higher input resistance (1.64 ± 0.24 GΩ vs. 0.56 ± 0.06 GΩ; $p = 0.0001$). In contrast, we did not find differences in cell capacitance (35.7 ± 3.7 pF vs. 36.2 ± 2.8 pF; $p = 0.91$). However, even though abGCs at 6 weeks exhibited a hyperpolarized RMP and lower input resistance they had a higher maximum frequency of firing in response to current stimuli (2 weeks = 17.8 ± 2.3 Hz; 6 weeks = 32.3 ± 2.8 Hz; $p = 0.0005$). Accordingly, a linear fitting to the input–output function revealed a shallower slope for older abGCs (2 weeks = 0.73 ± 0.09 Hz/pA; 6 weeks = 0.29 ± 0.03 Hz/pA; $p = 0.00003$; **Figure 1C**), suggesting a change in gain function as abGCs mature. In addition to changes in excitability due to intrinsic membrane properties, there were marked changes in the spontaneous excitatory postsynaptic currents (sEPSCs) as the abGC matured (**Supplementary Figure 1**). The frequency of sEPSCs increased by twofold with the maturation of the abGCs (2 weeks = 2.8 ± 0.7 Hz; 6 weeks = 6.8 ± 1.5 Hz; $p = 0.03$; **Supplementary Figures 1A,B**), together with an increase in the average amplitude of the sEPSCs (2 weeks = 10.1 ± 0.5 pA, 6 weeks = 13.9 ± 1.3 pA; $p = 0.02$). Lastly, both the rise and decay times of the EPSCs decreased with cell age (rise time, 2 weeks = 1.7 ± 0.1 ms, 6 weeks = 1.1 ± 0.08 ms; $p = 0.0001$; decay, 2 weeks = 6.8 ± 0.3 ms, 6 weeks = 5.1 ± 0.4 ms; $p = 0.003$). Together, these results indicate that as abGCs functionally integrate, between 2 and 6 weeks of cell age, the apparent decrease in excitability is offset by a large increase in the number of excitatory inputs, which exhibit distinct kinetic properties.

Adult-born granule cells exhibit I_h

Previously, we described the presence of I_h in GCs labeled born just after birth (P1–P6) and found that this current increased in amplitude during postnatal maturation (Hu et al., 2016); therefore, we examined the presence of I_h in abGCs. As shown in **Figure 2A**, stepping to negative potentials (-60 to -130 mV), revealed a characteristic inward current at both 2 and 6 weeks; however, at -130 mV the I_h was ~40% greater at 6 weeks (2 weeks = -72.9 ± 9.6 pA, $n = 17$ cells; 6 weeks = -101.4 ± 9.4, $n = 18$ cells; $p = 0.03$). Because the subunit composition of hyperpolarization-activated cyclic nucleotide-gated (HCN) channels determines the kinetic properties and voltage dependency of the currents (Zagotta et al., 2003; Shah, 2014), we examined the activation kinetics and the voltage-dependency of I_h at both ages. The rate of activation and the voltage-dependency were not different at these two time points (τ; 2 weeks = 57.3 ± 11.1 ms, 6 weeks = 53.7 ± 9.6 ms, $p = 0.8$; V_{half}: 2 weeks = -98.8 ± 1.2 mV, 6 weeks = -100.2 ± 2.2 mV; $p = 0.6$; **Figure 2B**). These results indicate that abGCs, like postnatal born GCs (Hu et al., 2016), exhibit an age-dependent increase in I_h, with no change in the kinetic properties.

Adrenergic modulation of I_h in adult-born GCs

Previous studies have shown that NA can regulate I_h through the activation of α_2-AR, which through a G_i-coupled pathway reduces cAMP and leads to a reduction in I_h (Umemura et al., 1986; Barth et al., 2008). To examine the possibility that NA acts directly in abGCs to regulate I_h, as opposed to a disynaptic effect, we conducted experiments in the presence of blockers of synaptic transmission and voltage-dependent sodium channels (10 μM CNQX, 50 μM APV, 10 μM GBZ, 0.5 μM TTX). Under these conditions, NA reduced I_h by approximately 20% the normalized current (at -130 mV), in both 2 and 6 weeks old abGCs (2 weeks = 0.77 ± 0.06, $n = 5$ cells, $p = 0.07$; 6 weeks = 0.82 ± 0.03; $n = 4$ cells; $p = 0.02$; **Figure 3A**). Importantly, application of the selective α_2-AR agonist, clonidine (Clon, 10 μM), similarly reduced I_h in abGCs, at both 2 and 6 weeks (2 weeks = 0.79 ± 0.06, $n = 6$ cells, $p = 0.03$; 6 weeks = 0.77 ± 0.04; $n = 7$ cells; $p = 0.001$; **Figure 3B**). To examine the possibility that the reduction in I_h by α_2-AR activation is due to changes in intracellular cAMP, we conducted additional pharmacological experiments in 6-week abGCs. Application of the membrane-permeable cAMP analog, 8-CPT-cAMP (8-CPT, 100 μM), increased I_h by 15% (normalized current, 1.15 ± 0.03; $n = 5$ cells; $p = 0.01$; **Figure 3B**), while pre-application of 8-CPT occluded the Clon-mediated suppression of I_h (normalized current, 0.93 ± 0.09; $n = 5$ cells; $p = 0.45$). In agreement with a regulation of the HCN by cAMP, Clon shifted the voltage–current relationship
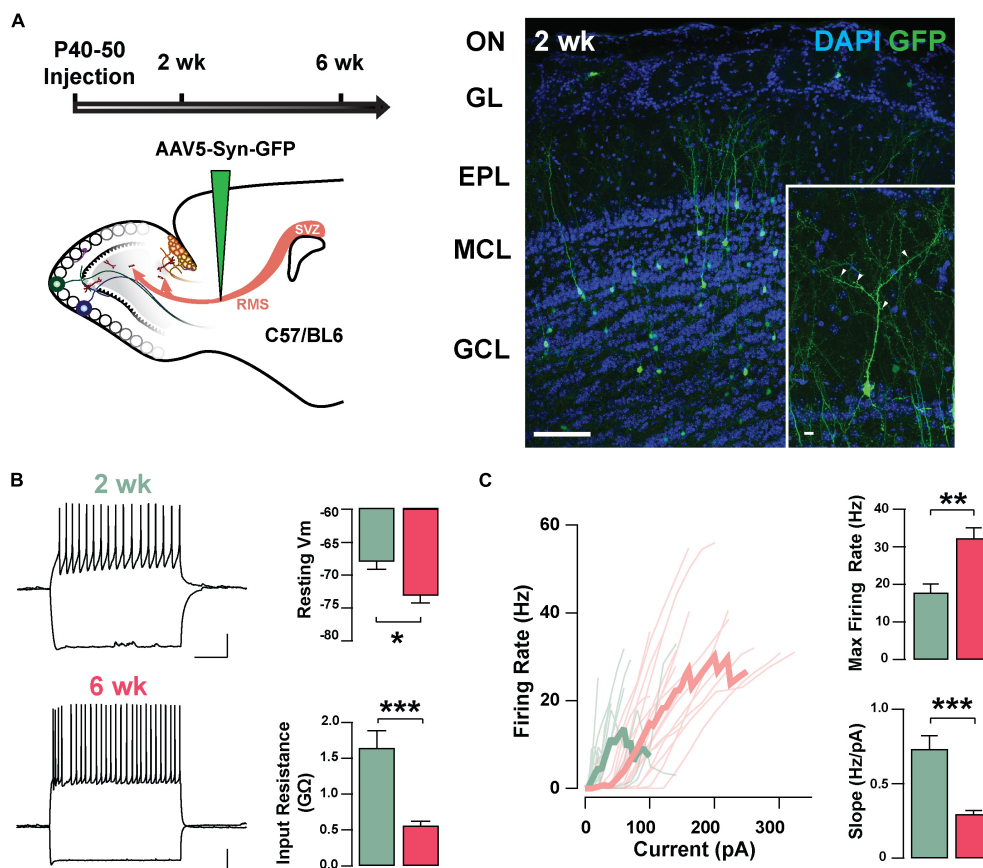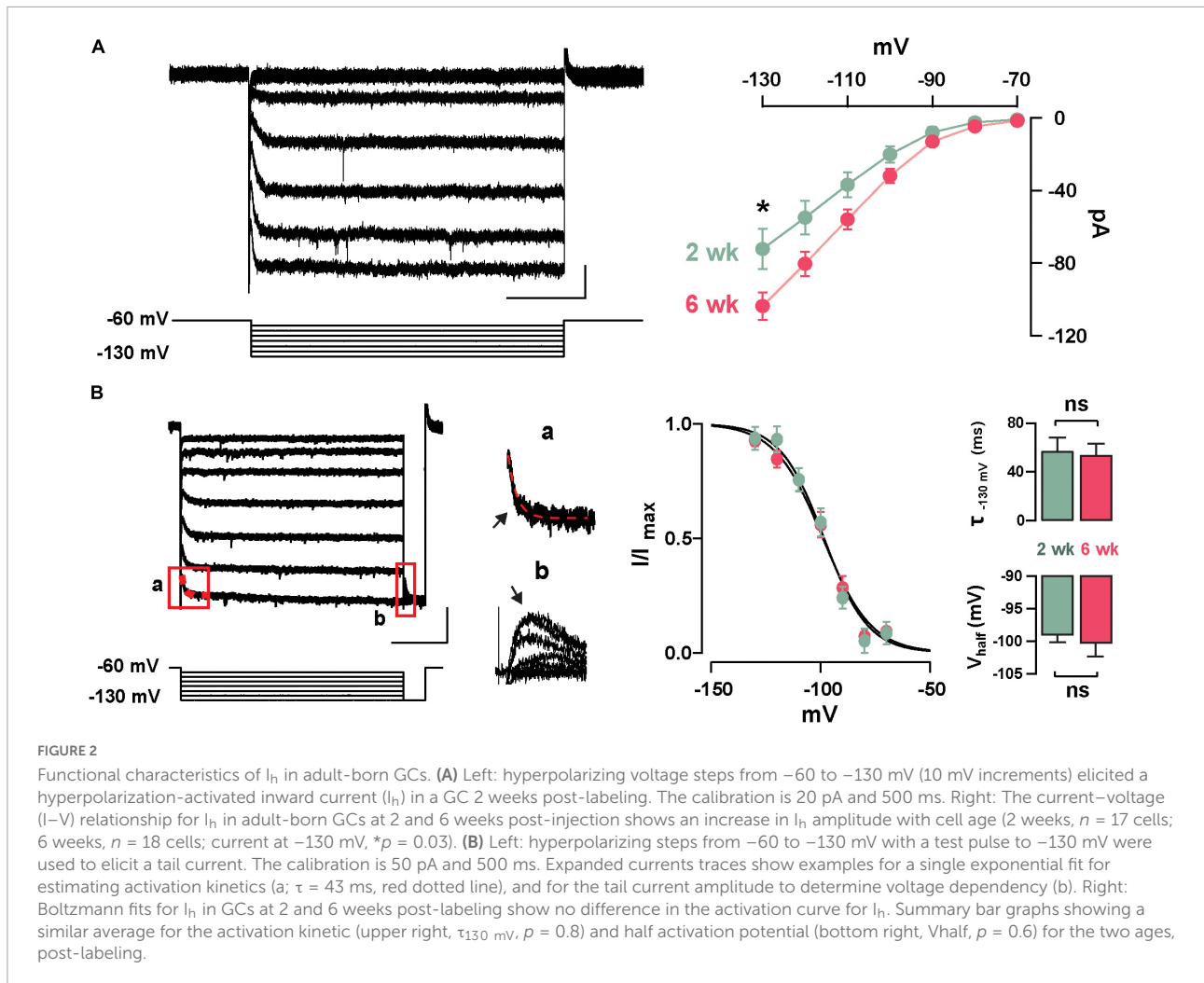
FIGURE 1

Intrinsic physiological properties of adult-born GCs. **(A)** Left: diagram of strategy used for labeling abGCs. Adult-born neurons were labeled with GFP at 40−50 days postnatal (p40−50) using virus-mediated transduction. We examined GC properties at 2 and 6 weeks (week) post-injection. Right: Confocal images of GFP-labeled adult-born neurons (green) in the MOB at 2 weeks post-injection. The inset shows a mature GC with a primary apical dendritic branch and abundant dendritic spines (arrow heads). OB cell layers, indicated on the left, were determined using DAPI (blue). Calibration: 100 and 10 μm (inset). **(B)** Left: traces from representative cells at 2 weeks (green) and 6 weeks (pink) post-injection showing responses to square current steps (−120 to +260 pA). The resting membrane potential (Vm) was −63 and −78 mV, respectively. The voltage traces show sustained action potentials in response to positive current injections and a small sag with negative current injections. The calibration is 20 mV and 500 ms. Right: bar graphs summarizing changes in GC excitability at two stages of cell maturation (2 weeks, $n = 16$ cells; 6 weeks, $n = 18$ cells). From 2 to 6 weeks post-injection, abGCs show a decrease in resting Vm (*$p = 0.003$), and a decrease in the input resistance (**$p = 0.0001$). **(C)** Left: input-output curves for firing rates elicited by a range of 2 s square current pulses. Right: Cells at 6 weeks post-labeling exhibited a higher maximal firing rate (**$p = 0.0005$), and lesser slope in their input-output function (***$p = 0.00003$).

of I_h to more negative potentials (V_{half}: Control = −98 ± 3.4 mV; Clon = −105.5 ± 3.4 mV, $p = 0.04$; **Figure 3C**), while the addition of 8-CPT shifted the V_{half} to more positive potentials (−94.4 ± 3.0 ms, $p = 0.02$). In contrast, the rate of activation of I_h at −130 mV did not change by α_2-AR activation or by the addition of 8-CPT (Control, CTL = 53.7 ± 9.5 ms; Clon = 47.7 ± 12.5 ms, $p = 0.16$; 8-CPT = 49.7 ± 14.2 ms; $p = 0.54$; **Figure 3D**). However, pre-application of the cAMP analog occluded the change in voltage dependency elicited by Clon (8CPT + Clon = −99.1 ± 4.2 mV, $p = 0.58$; **Figure 3E**). Lastly, in agreement with the decrease in I_h elicited by α_2-AR activation, Clon also produced an apparent increase in input resistance at both time points, albeit the effect was only significant at 6 weeks (fold-increase: 2 weeks = 1.29 ± 0.1,

$p = 0.08$; 6 weeks = 1.37 ± 0.08, $p = 0.01$; not shown). Together, these results indicate that I_h is present as early as the critical period during the functional integration of abGCs. Importantly, NA acting through α_2-ARs can modulate I_h in abGCs indicating another cellular mechanism by which NA can regulate the intrinsic excitability of GCs in the OB (Smith et al., 2009; Zimnik et al., 2013).

I_h-mediated resonance in GCs is modulated by α_2-AR activation

We have previously shown that subthreshold resonance in the theta (θ) frequency range in postnatally born GCs relies

FIGURE 2
Functional characteristics of I_h in adult-born GCs. **(A)** Left: hyperpolarizing voltage steps from −60 to −130 mV (10 mV increments) elicited a hyperpolarization-activated inward current (I_h) in a GC 2 weeks post-labeling. The calibration is 20 pA and 500 ms. Right: The current–voltage (I−V) relationship for I_h in adult-born GCs at 2 and 6 weeks post-injection shows an increase in I_h amplitude with cell age (2 weeks, n = 17 cells; 6 weeks, n = 18 cells; current at −130 mV, *p = 0.03). **(B)** Left: hyperpolarizing steps from −60 to −130 mV with a test pulse to −130 mV were used to elicit a tail current. The calibration is 50 pA and 500 ms. Expanded currents traces show examples for a single exponential fit for estimating activation kinetics (a; τ = 43 ms, red dotted line), and for the tail current amplitude to determine voltage dependency (b). Right: Boltzmann fits for I_h in GCs at 2 and 6 weeks post-labeling show no difference in the activation curve for I_h. Summary bar graphs showing a similar average for the activation kinetic (upper right, $\tau_{130\ mV}$, p = 0.8) and half activation potential (bottom right, Vhalf, p = 0.6) for the two ages, post-labeling.
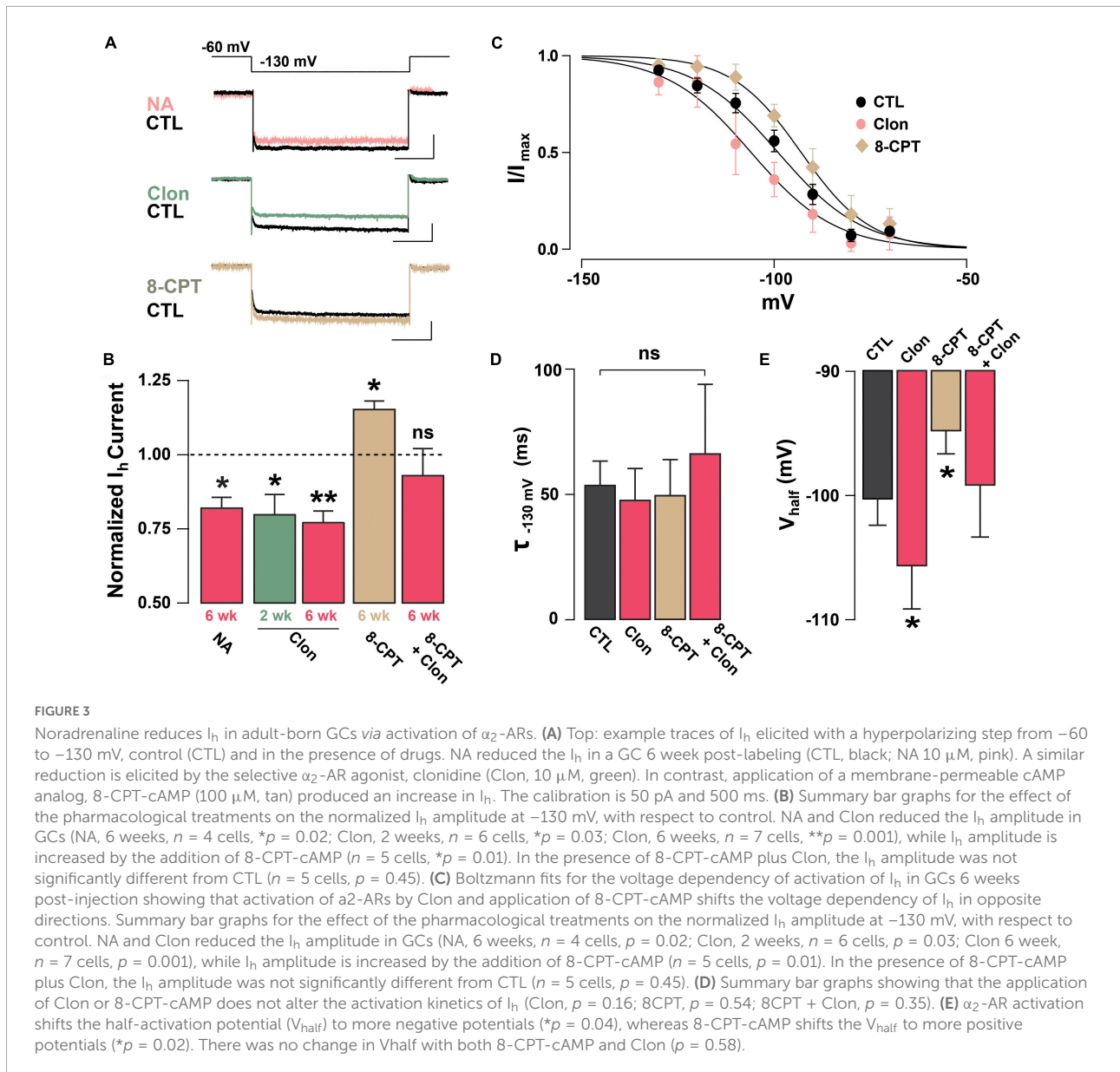
on I_h activation (Hu et al., 2016). Thus, we hypothesized that modulation of I_h by α_2-AR activation could regulate subthreshold resonance in mature GCs. A sinusoidal current stimulus of increasing frequency and constant amplitude injected into GCs (ZAP; see section "Materials and methods") revealed resonance in a subset of GCs in adult mice (**Figure 4A**). At −75 mV, the resonance strength (Q-factor) was 1.18 ± 0.06 and the resonant frequency (F_{res}) was 1.98 ± 0.28 Hz, consistent with data previously taken at similar membrane potentials in postnatal GCs (Hu et al., 2016). Clon produced a noticeable decrease in both the Q-factor and the F_{res} (1.05 ± 0.02; p < 0.02 and 1.00 ± 0.23 Hz; n = 6 cells; p < 0.0002; **Figure 4B**). Furthermore, Clon increased the input resistance of GCs, in a manner consistent with a reduction in I_h (control, 1.15 ± 0.16 GΩ vs. Clon, 2.31 ± 0.46 GΩ; n = 6 cells; p < 0.02, not shown). Additionally, 8-CPT-cAMP occluded the effect of Clon on both F_{res} and Q-factor (f_{res}, 8-CPT-cAMP, 1.10 ± 0.24 Hz vs. 8-CPT-cAMP + Clon, 1.01 ± 0.32 Hz, p = 0.82; Q-factor, 8-CPT-cAMP, 1.07 ± 0.03 vs. 8-CPT-cAMP + Clon, 1.03 ± 0.02, p = 0.2; n = 3 cells) (**Supplementary Figure 2**). These results

indicate that activation of α_2-ARs by NA modulates the resonant properties of GC in a manner consistent with a reduction of intracellular cAMP.

α_2-AR activation modulates dendritic excitability in abGCs and reciprocal dendrodendritic inhibition

We hypothesize that I_h is a target for the regulation of dendritic excitability in GCs and therefore the modulation of DDI at GC-MC synapses. To this extent, we recorded GABAergic currents from MCs in symmetric chloride conditions and elicited DDI by briefly (50 ms) depolarizing MCs (–70 to 0 mV). To isolate the dendritic output from GCs, we performed these experiments in the presence of TTX (0.5 μM) and in 0 Mg^{2+}. Under these conditions, GABA release from GC dendrites is solely driven by the activation of both AMPA and NMDA receptors upon the release of glutamate from MCs. A depolarizing step (50 ms) elicited a large inward current, with

FIGURE 3

Noradrenaline reduces I_h in adult-born GCs *via* activation of α_2-ARs. **(A)** Top: example traces of I_h elicited with a hyperpolarizing step from -60 to -130 mV, control (CTL) and in the presence of drugs. NA reduced the I_h in a GC 6 week post-labeling (CTL, black; NA 10 μM, pink). A similar reduction is elicited by the selective α_2-AR agonist, clonidine (Clon, 10 μM, green). In contrast, application of a membrane-permeable cAMP analog, 8-CPT-cAMP (100 μM, tan) produced an increase in I_h. The calibration is 50 pA and 500 ms. **(B)** Summary bar graphs for the effect of the pharmacological treatments on the normalized I_h amplitude at -130 mV, with respect to control. NA and Clon reduced the I_h amplitude in GCs (NA, 6 weeks, $n = 4$ cells, *$p = 0.02$; Clon, 2 weeks, $n = 6$ cells, *$p = 0.03$; Clon, 6 weeks, $n = 7$ cells, **$p = 0.001$), while I_h amplitude is increased by the addition of 8-CPT-cAMP ($n = 5$ cells, *$p = 0.01$). In the presence of 8-CPT-cAMP plus Clon, the I_h amplitude was not significantly different from CTL ($n = 5$ cells, $p = 0.45$). **(C)** Boltzmann fits for the voltage dependency of activation of I_h in GCs 6 weeks post-injection showing that activation of a2-ARs by Clon and application of 8-CPT-cAMP shifts the voltage dependency of I_h in opposite directions. Summary bar graphs for the effect of the pharmacological treatments on the normalized I_h amplitude at -130 mV, with respect to control. NA and Clon reduced the I_h amplitude in GCs (NA, 6 weeks, $n = 4$ cells, $p = 0.02$; Clon, 2 weeks, $n = 6$ cells, $p = 0.03$; Clon 6 week, $n = 7$ cells, $p = 0.001$), while I_h amplitude is increased by the addition of 8-CPT-cAMP ($n = 5$ cells, $p = 0.01$). In the presence of 8-CPT-cAMP plus Clon, the I_h amplitude was not significantly different from CTL ($n = 5$ cells, $p = 0.45$). **(D)** Summary bar graphs showing that the application of Clon or 8-CPT-cAMP does not alter the activation kinetics of I_h (Clon, $p = 0.16$; 8CPT, $p = 0.54$; 8CPT + Clon, $p = 0.35$). **(E)** α_2-AR activation shifts the half-activation potential (V_{half}) to more negative potentials (*$p = 0.04$), whereas 8-CPT-cAMP shifts the V_{half} to more positive potentials (*$p = 0.02$). There was no change in Vhalf with both 8-CPT-cAMP and Clon ($p = 0.58$).

a slow decay (369 ± 43 ms, $n = 26$ cells), similar to the time course of DDI previously reported by us and others (Isaacson and Strowbridge, 1998; Schoppa et al., 1998; Villar et al., 2021). This current was completely blocked by the GABA$_A$ receptor antagonist, gabazine (GBZ, 10 μM; $n = 4$ cells; **Figure 5A**). Quantification of the transferred charge indicated that Clon produced a significant increase in DDI (CTL, -110.7 ± 17.5 pC, Clon, -157.6 ± 25.6 pC; $n = 10$ cells; $p = 0.01$; **Figure 5B**), with a slight increase, although not significant, in the rate of decay of the DDI current (CTL, 315 ± 57 ms, Clon, 479 ± 53; $p = 0.08$; not shown). Importantly, the selective I_h blocker ZD7288 (ZD, 10 μM) also increased DDI onto MCs (CTL, -83.1 ± 15.8 pC, ZD, -189.2 ± 37.7 pC, $n = 16$ cells, $p = 0.003$, **Figure 5B**). Furthermore, pre-application of ZD occluded the increase

in DDI by α_2-AR activation (ZD, -115.3 ± 22.6 pC, ZD + Clon, -138.4 ± 32.4 pC; $n = 7$ cells; $p = 0.14$; **Figure 5B**), suggesting that the α_2-mediated increase in DDI occurs *via* a suppression of I_h. We note that the measured charge in ZD shows higher variability as we selected cells that did not exhibit a large increase in DDI, allowing room for additional enhancement should the clonidine-mediated enhancement be an independent effect. Surprisingly, however, when we used a physiological concentration of external Mg^{2+} (1 mM), α_2-AR activation resulted in a decrease in DDI (CTL, -83.4 ± 9.4 pC, Clon, -60.2 ± 9.4, $n = 15$ cells, $p = 0.006$, **Figure 5C**); similarly, application of the I_h blocker also resulted in a small reduction in DDI (CTL, -66.4 ± 8.2 pC, ZD, -51.3 ± 5.0 pC; $n = 13$ cells; $p = 0.03$, **Figure 5C**). We reason that it is
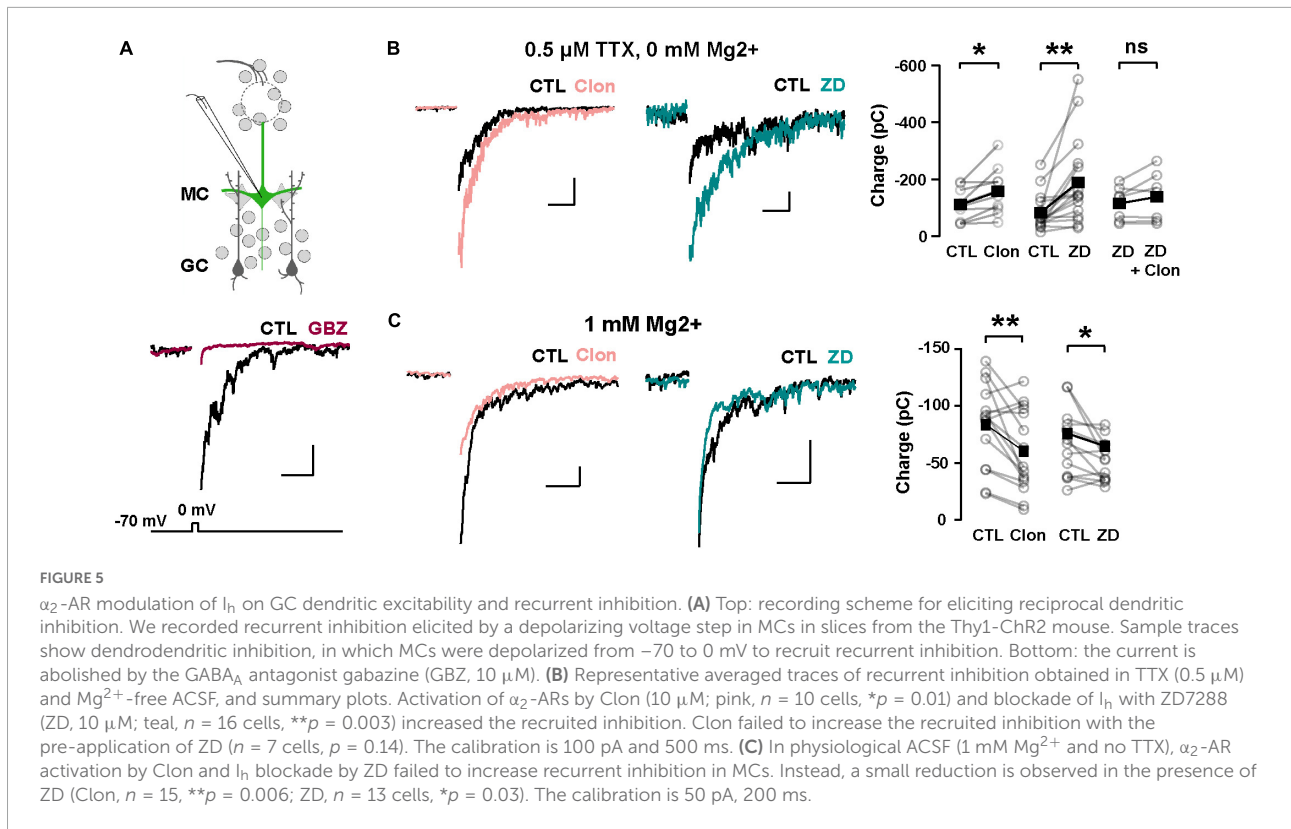
FIGURE 4

Activation of α_2-ARs decreases the resonance of GCs. **(A)** Top: Voltage responses (upper traces) to a ZAP current stimulus (lower traces) in a GC before (left) and after the application of Clon (10 μM, right). The calibration is 5 mV and 10 s; the ZAP stimulus amplitude is 5 pA (peak-to-peak). Bottom: impedance profiles for the trials shown in the figure above. In the control condition, the resonant strength (Q factor) is 1.45 and the peak frequency 2.83 Hz. In the presence of Clon (right), the resonant strength is 1.13 and the peak frequency is 1.73 Hz (right). The Vm was maintained at −75 mV for both trials. **(B)** Summary plots for the effect of Clon. Activation of α_2-ARs by the agonist significantly reduced both Q factor and resonant frequency (F_{res}) in GCs. *$p < 0.05$.

possible that under physiological blockade of NMDA receptors by Mg^{2+}, a suppression of I_h by α_2-AR activation could hyperpolarize the dendrites of GCs, as we previously showed (Hu et al., 2016), thus reducing the release of GABA from GCs.

α_2-AR suppression of I_h enhances lateral inhibition in the MOB

In addition to directly modulating recurrent inhibition at a given GC-MC synaptic pair, changes in GC dendritic excitability by I_h could alter lateral inhibition between MCs. To test this possibility, we elicited lateral inhibition in MCs using the Thy1-ChR2 mouse, in which the light-gated cation channel channelrhodopsin (ChR2) is expressed in MCs under the *Thy1* promoter (Arenkiel et al., 2007). In cell-attached configuration, we adjusted the light intensity so that a 2 ms light pulse reliably produced a single action potential in the MCs, with a short latency (under 5 ms, **Figure 6A**). We then recorded in voltage-clamp using a Cs-gluconate-based internal solution to isolate disynaptic lateral inhibition in the recorded MC from light-induced feedforward excitation. At −70 mV, light activation elicited a fast inward current (onset 6.3 ± 0.2 ms, not shown), while at the reversal potential for excitatory currents ($\sim$ +10 mV under the recording conditions), light stimulation produced a large outward current (249 ± 28 pA, $n = 41$ cells), that occurred with a longer delay (9.5 ± 0.2 ms, **Figure 6A**). In

physiological Mg^{2+}, the outward current had a faster decay (90.8 ± 12.9 ms) and was completely abolished by GBZ (10 μM; $n = 3$ cells; **Figure 6A**) consistent with the activation of dendrodendritic synapses from neighboring MCs. We note that at depolarized potentials (+10 mV), voltage-gated sodium and calcium channels are likely inactivated and therefore the outward current elicited by light stimulation is unlikely to result from recurrent inhibition from the recorded MCs. Therefore, the light-evoked disynaptic inhibition is likely to contain a predominant component from lateral inhibition.

Using this protocol to elicit lateral inhibition, we found that Clon produced an increase in the peak outward current (CTL, 212.1 ± 57.2 pA, Clon, 244.2 ± 61.5 pA; $n = 10$ cells; $p = 0.002$; **Figure 6B**), and the charge (CTL, 14.9 ± 2.6 pC, Clon, 19.5 ± 1.9 pC, $p = 0.04$), without affecting the rate of decay of the outward current (CTL, 141 ± 47 ms, vs. Clon, 99 ± 24 ms, $p = 0.44$). Similarly, blockade of I_h with ZD increased both the peak current and the transferred charge (CTL, 245.2 ± 39.7 pA, ZD, 304.6 ± 53.3 pA; $p = 0.002$; CTL, 13.2 ± 2.3 pC, ZD, 17.3 ± 3.1 pC; $p = 0.02$; $n = 13$ cells; **Figure 6B**). As with the recurrent inhibition in 0 mM external Mg^{2+}, pre-application of ZD occluded the increase in lateral inhibition elicited by α_2-AR activation (ZD, 313.7 ± 64.7 pA, ZD + Clo, 297.7 ± 64.4 pA; $p = 0.30$; ZD, 19.2 ± 4.0 pC, ZD + Clon, 23.7 ± 4.0 pC, $p = 0.09$; $n = 11$ cells; **Figure 6B**). These results indicate that suppression of I_h by α_2-AR activation can increase the amplitude of lateral inhibition, similar to the observed increase

FIGURE 5

α_2-AR modulation of I_h on GC dendritic excitability and recurrent inhibition. **(A)** Top: recording scheme for eliciting reciprocal dendritic inhibition. We recorded recurrent inhibition elicited by a depolarizing voltage step in MCs in slices from the Thy1-ChR2 mouse. Sample traces show dendrodendritic inhibition, in which MCs were depolarized from −70 to 0 mV to recruit recurrent inhibition. Bottom: the current is abolished by the GABA$_A$ antagonist gabazine (GBZ, 10 μM). **(B)** Representative averaged traces of recurrent inhibition obtained in TTX (0.5 μM) and Mg^{2+}-free ACSF, and summary plots. Activation of α_2-ARs by Clon (10 μM; pink, n = 10 cells, *p = 0.01) and blockade of I_h with ZD7288 (ZD, 10 μM; teal, n = 16 cells, **p = 0.003) increased the recruited inhibition. Clon failed to increase the recruited inhibition with the pre-application of ZD (n = 7 cells, p = 0.14). The calibration is 100 pA and 500 ms. **(C)** In physiological ACSF (1 mM Mg^{2+} and no TTX), α_2-AR activation by Clon and I_h blockade by ZD failed to increase recurrent inhibition in MCs. Instead, a small reduction is observed in the presence of ZD (Clon, n = 15, **p = 0.006; ZD, n = 13 cells, *p = 0.03). The calibration is 50 pA, 200 ms.

in GC dendritic output in the experiments described above in TTX and Mg^{2+}-free (**Figure 5B**).

The increase in lateral inhibition in MCs by α_2-AR activation likely results from an increase in inhibition from GC to MC rather than an increase in excitatory transmission MC-GC, as Clon did not affect the evoked EPSCs on GCs, recorded at −70 mV (peak current, CTL, −33.1 ± 7.7 pA, Clon, −25.7 ± 6.1 pA; p = 0.39; charge, CTL, −1.12 ± 0.20 pC, Clon, −0.91 ± 0.28 pC; p = 0.39; n = 5 cells; **Supplementary Figure 3**). A similar result was obtained with ZD (peak current, CTL, −50.6 ± 14.6 pA, ZD, −56.9 ± 20.2 pA, p = 0.59; charge, CTL, −1.69 ± 0.62 pC, ZD, −1.76 ± 0.62 pC; p = 0.73; n = 5 cells). In summary, these results indicate that modulation of I_h by α_2-AR modulation results from an increase in transmission at GC-MC synapses.

Discussion

The control of dendritic excitability in GCs is crucial for regulating dendrodendritic interactions with MCs, with both reciprocal and lateral inhibition affecting the spatiotemporal decorrelation of MC spiking activity in the OB (Wiechert et al., 2010; Gschwend et al., 2015; Wanner and Friedrich, 2020). These forms of inhibition are regulated by state-dependent noradrenergic modulation from the locus coeruleus (LC); however, beyond the description of changes in excitability in some cell types of the OB, the mechanisms of this regulation

are poorly understood (Jahr and Nicoll, 1982; Shipley et al., 1985; Trombley and Shepherd, 1992; Nai et al., 2009; Zimnik et al., 2013). Furthermore, inhibitory circuits within the OB undergo an exceptional remodeling throughout life due to the neurogenesis of GCs through a highly regulated process (Lledo and Saghatelyan, 2005; Lepousez et al., 2013; Gheusi and Lledo, 2014), including regulation by NA (Jahr and Nicoll, 1982; Veyrac et al., 2009; Fletcher and Chen, 2010; Moreno et al., 2012). Here, we provide evidence that NA, acting on α_2-ARs, can regulate the excitability of abGCs by reducing I_h *via* a cAMP-dependent mechanism. This suppression of I_h increases dendritic excitability, thereby enhancing lateral inhibition onto MCs and modulating the resonance of GCs. Together, these findings provide a novel mechanism by which adrenergic modulation of intrinsic properties of abGCs can regulate olfactory function in a state-dependent manner.

While prior studies have examined the progression of intrinsic and synaptic properties of abGCs in the OB as they matured, their primary focus was on earlier developmental time points leading up to 2–3 weeks of cell age (Belluzzi et al., 2003; Carleton et al., 2003). Here, we show that abGCs undergo further electrophysiological changes past this critical period with changes in basic electrophysiological parameters that result in a general decrease in intrinsic excitability between 3 and 6 weeks of age. These changes can provide a mechanism for the observed changes in odor tuning and response profiles
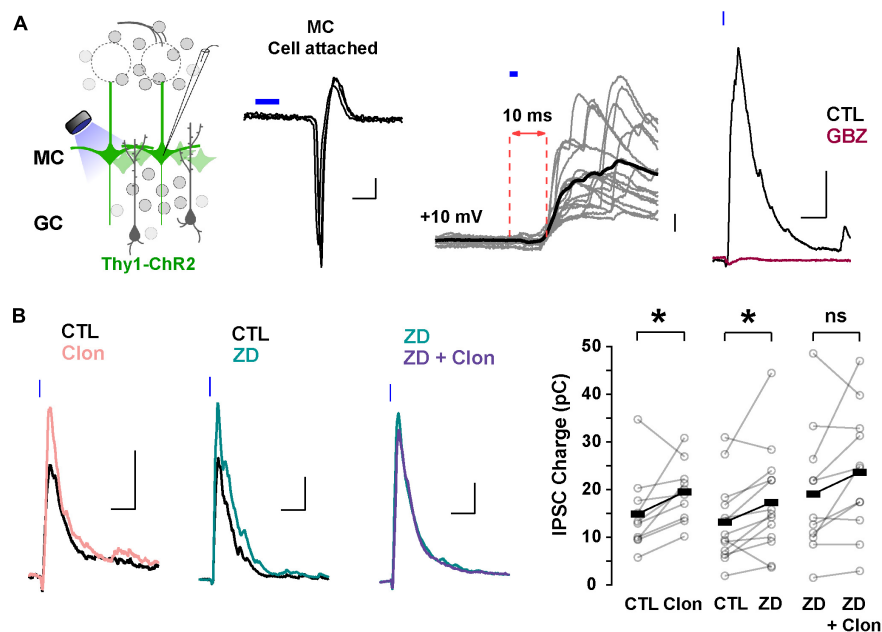
FIGURE 6

Suppression of I_h by α_2-AR increases lateral inhibition onto MCs. **(A)** Left: diagram of the strategy used to elicit lateral inhibition. We recorded from and optogenetically activated MCs expressing the ChR2 protein (Thy1-ChR2 mouse). Right: example of a cell-attached recording showing that activation of ChR2 (2 ms) elicits direct, reliable action potentials in the recorded MC. In voltage-clamp recordings at +10 mV, ChR2 stimulation evokes a disynaptic inhibitory current (10 ms delay) which is abolished by GBZ (10 μM, brown). The calibration is: cell-attached, 20 pA, 2 ms; whole cell, 50 pA, 50 ms. **(B)** Representative averaged traces (left) and summary plots (right) showing that α_2-AR activation by Clon and blockade of I_h increased the light-evoked inhibitory currents (Clon, pink, $n = 10$, *$p = 0.04$; ZD, teal, $n = 13$ cells, *$p = 0.02$). In the presence of ZD, Clon failed to increase the light-evoked inhibitory currents (purple; $n = 11$ cells, $p = 0.09$).

in adult-born neurons as a function of maturation (Magavi et al., 2005; Kovalchuk et al., 2015; Quast et al., 2017; Wallace et al., 2017). In addition, the increase in synaptic activity we observed, as abGCs matured beyond 2 weeks, aligns with previous studies showing an increase in the number of MC-GC synapses during development and changes in the relative expression of glutamatergic receptors such AMPA and NMDA receptors as GC mature (Hinds and Hinds, 1976; Carleton et al., 2003; Dietz et al., 2011). Interestingly, the changes in intrinsic excitability, in particular the expression of I_h, mirrored those of postnatally born neurons previously described (Hu et al., 2016), suggesting that in terms of I_h expression, adult neurogenesis recapitulates developmental or postnatal neurogenesis. Last, as we did not observe a cell-age difference in the I_h kinetics, we believe that the increase in current size is due to an increase in channel number, especially taking into account that we did not find a significant difference in average cell capacitance between both age groups. Further studies will examine this possibility.

The voltage dependency and activation kinetics of HCN channels are modulated by intracellular levels of cAMP, implicating I_h in the regulation of state-dependent network activity by neuromodulators that regulate cAMP concentrations such as NA (McCormick et al., 1991; Lüthi and McCormick, 1998; Surges et al., 2006; He et al., 2014). Our studies indicate the presence of α_2-ARs in abGCs and that their activation

produced modulation of I_h, as early as 2 weeks post-labeling in the RMS. Furthermore, abGCs during their functional stages of integration exhibit an α_2-AR-mediated reduction of I_h, by shifting the voltage dependency to lower membrane potentials, likely through reducing intracellular levels of cAMP. This agrees with our results showing that bath application of 8-CPT occluded the α_2-mediated suppression of I_h relative to control conditions, as well as shifting its voltage-dependency in abGCs.

α_2-mediated changes in I_h also reduced resonance in GCs. While it is unclear the effect that this decrease in resonance will have on odor processing in the OB, inputs into the MOB are driven by respiration, which occurs in the θ frequency domain, potentially allowing increased excitation of GCs at θ frequencies through this bandpass mechanism, thus altering the timing of GC to MC inhibition. Furthermore, the reduction in the resonance of GCs by α_2-AR activation may affect the temporal integration of excitatory inputs into the dendrites of GC. Studies in the hippocampus have shown that I_h can act as a bandpass filter, allowing synaptic inputs at θ frequencies to be preferentially transferred to the soma (Narayanan and Johnston, 2008).

Our experimental paradigm allowed us to examine the neuromodulation by NA of reciprocal and lateral inhibition in isolation. Previous studies of dendrodendritic inhibition have often used MC depolarization to elicit recurrent inhibition

(Isaacson and Strowbridge, 1998; Isaacson, 2001), or glomerular stimulation (Schoppa et al., 1998; Schoppa, 2006; Pressler et al., 2007), which fails to distinguish the contribution of reciprocal and lateral inhibition. Surprisingly, the effect of NA in reciprocal inhibition was Mg^{2+}-sensitive. In the absence of Mg^{2+}, α_2-AR activation and blockade of I_h increased the GABAergic output from GCs. However, in the presence of physiological Mg^{2+}, we observed the opposite effect. We hypothesize that the α_2-AR suppression of I_h would not only increase spine or dendrite resistance but could also hyperpolarize these compartments (Hu et al., 2016). In agreement, a similar effect has been observed in pre-synaptic compartments such as the calyx of Held (Huang and Trussell, 2014). At the level of the GC dendritic arbors or a dendritic spine, the increased resistance from the suppression of I_h allows for larger changes in voltage with glutamate receptor activation. This agrees with other studies showing an increase in dendritic excitability with α_2-AR suppression of I_h in pyramidal neurons (Barth et al., 2007, 2008; Wang et al., 2007; Labarrera et al., 2018). However, in GCs, the concurrent hyperpolarization induced by suppression of I_h would also shift the membrane potential farther from the voltage threshold for the release of the Mg^{2+} block in the NMDA receptors, as the α_2-mediated increase in reciprocal inhibition was observed only in the absence of Mg^{2+}. As GCs are not the sole source of lateral inhibition, potential excitation of external tufted cells and subsequently glomerular interneurons as part of the Thy1-ChR2 stimulations could also result in a di-synaptic inhibition onto MCs. Similar to our findings, periglomerular cells also exhibited a reduction in I_h and a membrane hyperpolarization with Clon application (Pignatelli et al., 2013).

At a circuit level, the enhancement of lateral, but not reciprocal inhibition, by α_2-ARs may coordinate MC output to enhance pattern separation of MC activity, which could result in the narrowing of odor tuning curves in MCs (Yokoi et al., 1995). As α_2-ARs exhibit the highest binding affinity to NA (Molinoff, 1984; Atzori et al., 2016; Ritter et al., 2019), we hypothesize that during behavioral states involving low LC activity, such as a state of low arousal, in which the animal is awake but not actively engaged in a task, the predominant action of NA on the OB circuit could be mediated by α_2-ARs. The activation of this receptor could favor the enhancement of lateral inhibition over reciprocal inhibition, and further enhance the signal-to-noise ratio within the OB, by allowing MCs that receive greater sensory inputs to propagate their signals to the cortex, while laterally inhibiting weakly activated MCs.

Taken together, our results show that NA can modulate the inhibitory functions of GCs *via* the regulation of I_h. Due to the observed physiological differences between young and old abGCs, future studies will address the neuromodulation of dendritic computation in an age-dependent manner.

Data availability statement

The original contributions presented in this study are included in the article/Supplementary material, further inquiries can be directed to the corresponding author.

Ethics statement

This animal study was reviewed and approved by the IACUC of the University of Maryland, College Park.

Author contributions

RH and RA designed the research. RH, JS, GD, and PV performed the research and analyzed the data. RH, JS, PV, and RA wrote the manuscript. All authors contributed to the article and approved the submitted version.

Funding

Conflict of interest

The authors declare that the research was conducted in the absence of any commercial or financial relationships that could be construed as a potential conflict of interest.

Publisher's note

All claims expressed in this article are solely those of the authors and do not necessarily represent those of their affiliated organizations, or those of the publisher, the editors and the reviewers. Any product that may be evaluated in this article, or claim that may be made by its manufacturer, is not guaranteed or endorsed by the publisher.

Supplementary material

The Supplementary Material for this article can be found online at: https://www.frontiersin.org/articles/10.3389/fncel.2022.1055569/full#supplementary-material

References

Altman, J. (1962). Are new neurons formed in the brains of adult mammals? *Science (New York, N.Y.)* 135, 1127–1128. doi: 10.1126/science.135.3509.1127

Altman, J., and Das, G. D. (1965). Post-natal origin of microneurones in the rat brain. *Nature* 207, 953–956. doi: 10.1038/207953a0

Arenkiel, B. R., Peca, J., Davison, I. G., Feliciano, C., Deisseroth, K., Augustine, G. J. J., et al. (2007). In Vivo light-induced activation of neural circuitry in transgenic mice expressing channelrhodopsin-2. *Neuron* 54, 205–218. doi: 10.1016/j.neuron.2007.03.005

Atzori, M., Cuevas-Olguin, R., Esquivel-Rendon, E., Garcia-Oscos, F., Salgado-Delgado, R. C., Saderi, N., et al. (2016). Locus ceruleus norepinephrine release: A central regulator of CNS spatio-temporal activation? *Front. Synaptic Neurosci.* 8:25. doi: 10.3389/fnsyn.2016.00025

Barth, A. M. I., Vizi, E. S., and Lendvai, B. (2007). Noradrenergic enhancement of Ca2+ responses of basal dendrites in layer 5 pyramidal neurons of the prefrontal cortex. *Neurochem. Int.* 51, 323–327. doi: 10.1016/j.neuint.2007.05.008

Barth, A. M. I., Vizi, E. S., Zelles, T., and Lendvai, B. (2008). α 2 -Adrenergic receptors modify dendritic spike generation via HCN channels in the prefrontal cortex. *J. Neurophysiol.* 99, 394–401. doi: 10.1152/jn.00943.2007

Belluzzi, O., Benedusi, M., Ackman, J., and LoTurco, J. J. (2003). Electrophysiological differentiation of new neurons in the olfactory bulb. *J. Neurosci.* 23, 10411–10418. doi: 10.1371/journal.pone.0037742

Berridge, C. W., and Waterhouse, B. D. (2003). The locus coeruleus-noradrenergic system: Modulation of behavioral state and state-dependent cognitive processes. *Brain Res. Rev.* 42, 33–84. doi: 10.1016/S0165-0173(03)00143-7

Boyd, A. M., Sturgill, J. F., Poo, C., and Isaacson, J. S. (2012). Cortical feedback control of olfactory bulb circuits. *Neuron* 76, 1161–1174. doi: 10.1016/j.neuron.2012.10.020

Carleton, A., Petreanu, L. T., Lansford, R., Alvarez-Buylla, A., and Lledo, P. M. (2003). Becoming a new neuron in the adult olfactory bulb. *Nat. Neurosci.* 6, 507–518. doi: 10.1038/nn1048

Dietz, S. B., Markopoulos, F., and Murthy, V. N. (2011). Postnatal development of dendrodendritic inhibition in the mammalian olfactory bulb. *Front. Cell. Neurosci.* 5:10. doi: 10.3389/fncel.2011.00010

Fletcher, M. L., and Chen, W. R. (2010). Neural correlates of olfactory learning: Critical role of centrifugal neuromodulation. *Learn. Mem. (Cold Spring Harbor, N.Y.)* 17, 561–570. doi: 10.1101/lm.941510

Fukunaga, I., Herb, J. T., Kollo, M., Boyden, E. S., and Schaefer, A. T. (2014). Independent control of gamma and theta activity by distinct interneuron networks in the olfactory bulb. *Nat. Neurosci.* 17, 1208–1216. doi: 10.1038/nn.3760

Gheusi, G., and Lledo, P.-M. (2014). Adult neurogenesis in the olfactory system shapes odor memory and perception. *Prog. Brain Res.* 208, 157–175. doi: 10.1016/B978-0-444-63350-7.00006-1

Griffen, T. C., and Maffei, A. (2014). GABAergic synapses: Their plasticity and role in sensory cortex. *Front. Cell. Neurosci.* 8:1–22. doi: 10.3389/fncel.2014.00091

Gschwend, O., Abraham, N. M., Lagier, S., Begnaud, F., Rodriguez, I., and Carleton, A. (2015). Neuronal pattern separation in the olfactory bulb improves odor discrimination learning. *Nat. Neurosci.* 208, 157–175. doi: 10.1038/nn.4089

Gutfreund, Y., Yarom, Y., and Segev, I. (1995). Subthreshold oscillations and resonant frequency in guinea-pig cortical neurons: Physiology and modelling. *J. Physiol.* 483, 621–640.

He, C., Chen, F., Li, B., and Hu, Z. (2014). Neurophysiology of HCN channels: From cellular functions to multiple regulations. *Prog. Neurobio.* 112, 1–23. doi: 10.1016/j.pneurobio.2013.10.001

Hinds, J. W., and Hinds, P. L. (1976). Synapse formation in the mouse olfactory bulb. *J. Comp. Neurol.* 169, 15–40.

Hu, R., Ferguson, K. A., Whiteus, C. B., Meijer, D. H., and Araneda, R. C. (2016). Hyperpolarization-activated currents and subthreshold resonance in granule cells of the olfactory bulb. *ENeuro* 3, ENEURO.197–ENEURO.116. doi: 10.1523/ENEURO.0197-16.2016

Huang, H., and Trussell, L. O. (2014). Presynaptic HCN channels regulate vesicular glutamate transport. *Neuron* 84, 340–346. doi: 10.1016/j.neuron.2014.08.046

Hutcheon, B., and Yarom, Y. (2000). Resonance, oscillation and the intrinsic frequency preferences of neurons. *Trends Neurosci.* 23, 2016–2222.

Isaacson, J. S. (2001). Mechanisms governing dendritic γ-aminobutyric acid (GABA) release in the rat olfactory bulb. *Proc. Natl. Acad. Sci. U.S.A.* 98, 337–342. doi: 10.1073/pnas.021445798

Isaacson, J. S., and Scanziani, M. (2011). How inhibition shapes cortical activity. *Neuron* 72, 231–243. doi: 10.1016/j.neuron.2011.09.027

Isaacson, J. S., and Strowbridge, B. W. (1998). Olfactory reciprocal synapses: Dendritic signaling in the CNS. *Neuron* 20, 749–761. doi: 10.1016/S0896-6273(00)81013-2

Jahr, C. E., and Nicoll, R. a (1980). Dendrodendritic inhibition: Demonstration with intracellular recording. *Science* 207, 1473–1475. doi: 10.1126/science.7361098

Jahr, C. E., and Nicoll, R. a (1982). Noradrenergic modulation of dendrodendritic inhibition in the olfactory bulb. *Nature* 297, 227–229. doi: 10.1038/297227a0

Kovalchuk, Y., Homma, R., Liang, Y., Maslyukov, A., Hermes, M., Thestrup, T., et al. (2015). In vivo odourant response properties of migrating adult-born neurons in the mouse olfactory bulb. *Nat. Commun.* 6, 1–2. doi: 10.1038/ncomms7349

Labarrera, C., Deitcher, Y., Dudai, A., Weiner, B., Kaduri Amichai, A., Zylbermann, N., et al. (2018). Adrenergic modulation regulates the dendritic excitability of layer 5 pyramidal neurons in Vivo. *Cell Rep.* 23, 1034–1044. doi: 10.1016/j.celrep.2018.03.103

Lepousez, G., and Lledo, P.-M. (2013). Odor discrimination requires proper olfactory fast oscillations in awake mice. *Neuron* 80, 1010–1024. doi: 10.1016/j.neuron.2013.07.025

Lepousez, G., Nissant, A., and Lledo, P. M. (2015). Adult neurogenesis and the future of the rejuvenating brain circuits. *Neuron* 86, 387–401. doi: 10.1016/j.neuron.2015.01.002

Lepousez, G., Valley, M. T., and Lledo, P.-M. (2013). The impact of adult neurogenesis on olfactory bulb circuits and computations. *Ann. Rev. Physiol.* 75, 339–363. doi: 10.1146/annurev-physiol-030212-183731

Lledo, P., Gheusi, G., and Vincent, J. (2005). Information processing in the mammalian olfactory system. *Physiol. Rev.* 85, 281–317. doi: 10.1152/physrev.00008.2004

Lledo, P.-M., Alonso, M., and Grubb, M. S. (2006). Adult neurogenesis and functional plasticity in neuronal circuits. *Nat. Rev. Neurosci.* 7, 179–193. doi: 10.1038/nrn1867

Lledo, P.-M., and Saghatelyan, A. (2005). Integrating new neurons into the adult olfactory bulb: Joining the network, life-death decisions, and the effects of sensory experience. *Trends Neurosci.* 28, 248–254. doi: 10.1016/j.tins.2005.03.005

Lois, C., and Alvarez-Buylla, A. (1994). Long-distance neuronal migration in the adult mammalian brain. *Science* 264, 1145–1148. doi: 10.1126/science.8178174

Lüthi, A., and McCormick, D. A. (1998). H-Current: Properties of a neuronal and network pacemaker. *Neuron* 21, 9–12.

Magavi, S. S. P., Mitchell, B. D., Szentirmai, O., Carter, B. S., and Macklis, J. D. (2005). Adult-born and preexisting olfactory granule neurons undergo distinct experience-dependent modifications of their olfactory responses in vivo. *J. Neurosci.* 25, 10729–10739. doi: 10.1523/JNEUROSCI.2250-05.2005

Markopoulos, F., Rokni, D., Gire, D., and Murthy, V. (2012). Functional properties of cortical feedback projections to the olfactory bulb. *Neuron* 76, 1175–1188. doi: 10.1016/j.neuron.2012.10.028

McCormick, D. A., Pape, H. C., and Williamson, A. (1991). Actions of norepinephrine in the cerebral cortex and thalamus: Implications for function of the central noradrenergic system. *Prog. Brain Res.* 88, 293–305. doi: 10.1016/S0079-6123(08)63817-0

Molinoff, P. B. (1984). α- and β-Adrenergic receptor subtypes: Properties. Distribution and regulation. *Drugs* 28, 1–15. doi: 10.2165/00003495-198400282-00002

Moreno, M. M., Bath, K., Kuczewski, N., Sacquet, J., Didier, a, and Mandairon, N. (2012). Action of the noradrenergic system on adult-born cells is required for olfactory learning in mice. *J. Neurosci.* 32, 3748–3758. doi: 10.1523/JNEUROSCI.6335-11.2012

Nai, Q., Dong, H.-W., Hayar, A., Linster, C., and Ennis, M. (2009). Noradrenergic regulation of GABAergic inhibition of main olfactory bulb mitral cells varies as a function of concentration and receptor subtype. *J. Neurophysiol.* 101, 2472–2484. doi: 10.1152/jn.91187.2008

Narayanan, R., and Johnston, D. (2008). The h channel mediates location dependence and plasticity of intrinsic phase response in rat hippocampal neurons. *J. Neurosci.* 28, 5846–5860. doi: 10.1523/JNEUROSCI.0835-08.2008

Otazu, G., Chae, H., Davis, M., and Albeanu, D. (2015). Cortical feedback decorrelates olfactory bulb output in awake mice. *Neuron* 86, 1461–1477. doi: 10.1016/j.neuron.2015.05.023

Petreanu, L., and Alvarez-Buylla, A. (2002). Maturation and death of adult-born olfactory bulb granule neurons: Role of olfaction. *J. Neurosci.* 22, 6106–6113. doi: 20026588

Pignatelli, A., Borin, M., Fogli Iseppe, A., Gambardella, C., and Belluzzi, O. (2013). The h-current in periglomerular dopaminergic neurons of the mouse olfactory bulb. *PLoS One* 8:e56571. doi: 10.1371/journal.pone.0056571

Pressler, R. T., Inoue, T., and Strowbridge, B. W. (2007). Muscarinic receptor activation modulates granule cell excitability and potentiates inhibition onto mitral cells in the rat olfactory bulb. *J. Neurosci.* 27, 10969–10981. doi: 10.1523/JNEUROSCI.2961-07.2007

Quast, K., Ung, K., Froudarakis, E., Huang, L., Herman, I., Addison, A., et al. (2017). Developmental broadening of inhibitory sensory maps. *Nat. Neurosci.* 20, 189–199. doi: 10.1038/nn.4467

Ritter, J. M., Flower, R. J., Henderson, G., Loke, Y. K., MacEwan, D., Rang, H. P., et al. (2019). "Noradrenergic Transmission" in *Rang and Dale's Pharmacology*, 9th Edn. (Edinburgh: Elsevier), 197–198.

Sara, S. J. (2009). The locus coeruleus and noradrenergic modulation of cognition. *Nat. Rev. Neurosci.* 10, 211–223. doi: 10.1038/nrn2573

Schoppa, N. E. (2006). Synchronization of olfactory bulb mitral cells by precisely timed inhibitory inputs. *Neuron* 49, 271–283. doi: 10.1016/j.neuron.2005.11.038

Schoppa, N. E., and Urban, N. N. (2003). Dendritic processing within olfactory bulb circuits. *Trends Neurosci.* 26, 501–506. doi: 10.1016/S0166-2236(03)00228-5

Schoppa, N. E., and Westbrook, G. L. (1999). Regulation of synaptic timing in the olfactory bulb by an A-type potassium current. *Nat. Neurosci.* 2, 1106–1113. doi: 10.1038/16033

Schoppa, N. E., Kinzie, J. M., Sahara, Y., Segerson, T. P., and Westbrook, G. L. (1998). Dendrodendritic inhibition in the olfactory bulb is driven by NMDA receptors. *J. Neurosci.* 18, 6790–6802.

Shah, M. M. (2014). Cortical HCN channels: Function, trafficking and plasticity. *J. Physiol.* 592, 2711–2719. doi: 10.1113/jphysiol.2013.270058

Shipley, M. T., Halloran, F. J., and de la Torre, J. (1985). Surprisingly rich projection from locus coeruleus to the olfactory bulb in the rat. *Brain Res.* 329, 294–299. doi: 10.1016/0006-8993(85)90537-2

Smith, R. S., Weitz, C. J., and Araneda, R. C. (2009). Excitatory actions of noradrenaline and metabotropic glutamate receptor activation in granule cells of the accessory olfactory bulb. *J. Neurophysiol.* 102, 1103–1114. doi: 10.1152/jn.91093.2008

Stroh, O., Freichel, M., Kretz, O., Birnbaumer, L., Hartmann, J., and Egger, V. (2012). NMDA Receptor-dependent synaptic activation of TRPC channels in olfactory bulb granule cells. *J. Neurosci.* 32, 5737–5746. doi: 10.1523/JNEUROSCI.3753-11.2012

Surges, R., Brewster, A. L., Bender, R. A., Beck, H., Feuerstein, T. J., and Baram, T. Z. (2006). Regulated expression of HCN channels and cAMP levels shape the properties of the h current in developing rat hippocampus. *Eur. J. Neurosci.* 24, 94–104. doi: 10.1111/j.1460-9568.2006.04880.x

Trombley, P. Q., and Shepherd, G. M. (1992). Noradrenergic inhibition of synaptic transmission between mitral and granule cells in mammalian olfactory bulb cultures. *J. Neurosci.* 12, 3985–3991.

Umemura, S., Smyth, D. D., and Pettinger, W. A. (1986). Alpha 2-adrenoceptor stimulation and cellular cAMP levels in microdissected rat glomeruli. *Am. J. Physiol. Renal Physiol.* 250, F103–F108. doi: 10.1152/ajprenal.1986.250.1.F103

Vera, J., Pezzoli, M., Pereira, U., Bacigalupo, J., and Sanhueza, M. (2014). Electrical resonance in the θ frequency range in olfactory amygdala neurons. *PLoS One* 9:e85826. doi: 10.1371/journal.pone.0085826

Veyrac, A., Sacquet, J., Nguyen, V., Marien, M., Jourdan, F., and Didier, A. (2009). Novelty determines the effects of olfactory enrichment on memory and neurogenesis through noradrenergic mechanisms. *Neuropsychopharmacology* 34, 786–795. doi: 10.1038/npp.2008.191

Villar, P. S., Hu, R., and Araneda, R. C. (2021). Long-range GABAergic inhibition modulates spatiotemporal dynamics of the output neurons in the olfactory bulb. *J. Neurosci.* 41, 3610–3621. doi: 10.1523/JNEUROSCI.1498-20.2021

Wallace, J. L., Wienisch, M., and Murthy, V. N. (2017). Development and refinement of functional properties of adult-born neurons. *Neuron* 96, 883.e–896.e. doi: 10.1016/j.neuron.2017.09.039

Wang, M., Ramos, B. P., Paspalas, C. D., Shu, Y., Simen, A., Duque, A., et al. (2007). α2A-Adrenoceptors strengthen working memory networks by inhibiting cAMP-HCN channel signaling in prefrontal cortex. *Cell* 129, 397–410. doi: 10.1016/j.cell.2007.03.015

Wanner, A. A., and Friedrich, R. W. (2020). Whitening of odor representations by the wiring diagram of the olfactory bulb. *Nat. Neurosci.* 23, 433–442. doi: 10.1038/s41593-019-0576-z

Wiechert, M. T., Judkewitz, B., Riecke, H., and Friedrich, R. W. (2010). Mechanisms of pattern decorrelation by recurrent neuronal circuits. *Nat. Neurosci.* 13, 1003–1010. doi: 10.1038/nn.2591

Yokoi, M., Mori, K., and Nakanishi, S. (1995). Refinement of odor molecule tuning by dendrodendritic synaptic inhibition in the olfactory bulb. *Proc. Natl. Acad. Sci. U.S.A.* 92, 3371–3375. doi: 10.1073/pnas.92.8.3371

Zagotta, W. N., Olivier, N. B., Black, K. D., Young, E. C., Olson, R., and Gouaux, E. (2003). Structural basis for modulation and agonist specificity of HCN pacemaker channels. *Nature* 425, 200–205. doi: 10.1038/nature01922

Zimnik, N. C., Treadway, T., Smith, R. S., and Araneda, R. C. (2013). α1A-Adrenergic regulation of inhibition in the olfactory bulb. *J. Physiol.* 591, 1631–1643. doi: 10.1113/jphysiol.2012.248591